

Control of excitonic absorption by thickness variation in few-layer GaSe

Arne Budweg¹, Dinesh Yadav¹, Alexander Grupp¹, Alfred Leitenstorfer¹, Maxim Trushin^{2,1},
Fabian Pauly^{3,1,*}, Daniele Brida^{1,+}

¹ Department of Physics and Center for Applied Photonics, University of Konstanz, D-78457
Konstanz, Germany

² Centre for Advanced 2D Materials, National University of Singapore, 6 Science Drive 2,
Singapore 117546

³ Okinawa Institute of Science and Technology Graduate University, Onna-son, Okinawa
904-0395, Japan

* email: fabian.pauly@oist.jp

+ email: daniele.brida@uni-konstanz.de

ABSTRACT

We control the thickness of GaSe on the level of individual layers and study the corresponding optical absorption via highly sensitive differential transmission measurements. Suppression of excitonic transitions is observed when the number of layers is smaller than a critical value of 8. Through ab-initio modelling we are able to assign this behavior to a fundamental change in the band structure that leads to the formation of a valence band shaped as an inverted Mexican hat in thin GaSe. This intrinsic modulation of the optical properties of GaSe provides attractive resources for the development of functional optoelectronic devices based on a single material.

Recent investigations of the electronic structure of layered materials have led to disruptive advances in photonics, optoelectronics and spintronics [1-6]. In this context, metal monochalcogenides form one subgroup with similar structural properties that allow thickness reduction down to atomically thin two-dimensional (2D) crystals with a great variety of unique qualities. GaSe is a prominent member of this group that is widely used in near- and mid-infrared nonlinear optics [7,8]. First studies using few-layer GaSe in transistors [9] and photodetectors [10,11] have been performed. Recent photoluminescence measurements on GaSe nanosheets demonstrated a high preservation of photon polarization between absorption and photoluminescence, indicating a high potential for spintronic applications [12,13]. Furthermore, theoretical calculations suggest carrier-induced magnetism in single-layer GaSe [14].

In this Letter, we demonstrate experimentally the possibility to control the excitonic absorption from substantial enhancement to complete suppression by changing the number of GaSe layers in a nanosheet. Based on theoretical modelling, the qualitative variation of the absorption properties is associated with the transition between bulk and 2D confinement of the electronic wavefunctions at a thickness of approximately 9 nm. At this value, the enhancement of Coulomb attraction within electrons-hole pairs competes with an inversion of the curvature of the valence band, strongly modulating light-matter coupling in few-layer flakes of GaSe.

In detail, GaSe is a III-VI semiconductor, forming crystals with a hexagonal layered structure. Individual layers consist of four atomic planes in a Se-Ga-Ga-Se order and interlayer bonding arises from weak van der Waals forces. In the ϵ -GaSe polytype the stacking follows an AB sequence, corresponding to the non-centrosymmetric space group D_{3h}^1 [15,16]. Thickness values between 0.8 and 1 nm are reported for a GaSe monolayer [13,17,18]. Figure 1 displays the crystal structure of a double layer of GaSe in side (a) and top (b) view, stacked according to the ϵ polytype. At room temperature, bulk GaSe exhibits a quasi-direct bandgap of

approximately 2 eV. The valence band maximum (VBM) is at the Γ point, while the global conduction band minimum (CBM) is positioned in proximity of the M point. However an almost isoenergetic local minimum exists at the Γ point, exceeding the M valley by only 10 meV [19]. The direct exciton with a binding energy of 19 meV is also located at the Γ point, in close energetic vicinity to the direct and indirect interband transitions [15,20].

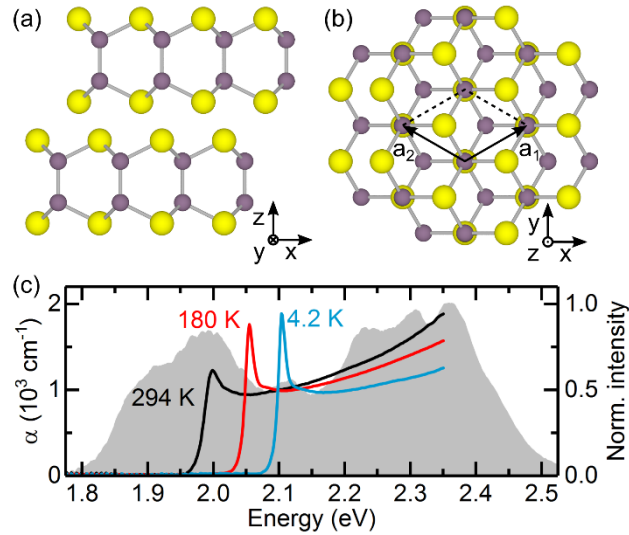


Fig 1: Schematic crystal structure of ϵ -GaSe viewed perpendicularly to the y - (a) and z -axis (b). Yellow and violet spheres represent selenium and gallium atoms, respectively. (c) Measured absorption coefficient for bulk ϵ -GaSe at different temperatures (solid lines) and normalized intensity spectrum of the pump pulses (gray area) employed in the transient absorption experiments.

All samples are fabricated by mechanical exfoliation of a Bridgman grown ϵ -GaSe single crystal. This material is first thinned down to a thickness of about 1 μm by successive exfoliation with adhesive tape. The flakes are then transferred to a 150 μm thick SiO_2 substrate. By continuing the exfoliation on the substrate, we produce large homogenous areas of few-layer GaSe with thicknesses down to 4 nm. Residual adhesive is removed by cleaning the surface with acetone and isopropanol. Some samples are additionally sputter-coated with a

15 nm protective layer of Si_3N_4 to exclude oxidation of GaSe at ambient conditions. All specimens are stored under nitrogen atmosphere.

Few-layer flakes are identified in an optical microscope. In addition, topographical characterization of the relevant areas on the sample is performed with an atomic force microscope (AFM) operating in tapping mode. Figures 2(a)–2(d) show AFM scans of four different regions with thicknesses ranging between 4 and 16 nm. In all maps, the white scale bars indicate a length of $10\ \mu\text{m}$. Height profiles along these lines are plotted in Fig. 2(e). Adopting a single-layer thickness between 0.8 and 1 nm [13,17,18], these values correspond to a number of layers between 4 and 20 for the four distinct specimens.

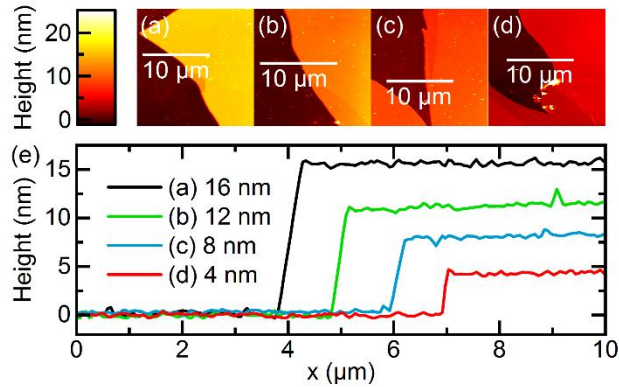


Fig 2: Topographical images of few-layer GaSe on SiO_2 . The height profiles taken along the white lines in panels (a)-(d) are depicted in panel (e), revealing thicknesses between 4 and 16 nm.

Transient absorption measurements of the samples are performed with an ultrafast laser system operating at a repetition rate of 50 kHz [21]. A custom-designed noncollinear optical parametric amplifier delivers pump pulses with a bandwidth of 0.52 eV at a central energy of 2.15 eV, as plotted in Fig. 1(c). These pulses are compressed to a temporal duration of 7 fs by means of customized dielectric chirped mirrors (DCMs). The pump-induced transmission change is probed by a white-light supercontinuum comprising spectral components between 1.7 and 2.8 eV at a pulse duration of 10 fs. Pump and probe pulses are focused onto the sample under a small angle to separate the beams after transmission through the sample.

Using an off-axis parabolic mirror with a focal length of 50.8 mm, we reach focus diameters of 30 μm for the pump and 15 μm for the probe beam while keeping the excitation density at a moderate value of 200 $\mu\text{J}/\text{cm}^2$. Orthogonal polarization between the beams enables us to filter out residual pump light before detection. The experiments are performed in a cryostat with the possibility to control the sample temperature down to 4.2 K. The probe light, collected after interaction with the sample, is spectrally dispersed and then detected by a fast CCD linear array [21] for the measurement of the differential transmission.

We have exploited the same broadband probe beam to also determine the linear absorption spectra of a 25 μm thick free-standing GaSe crystal mounted inside the cryostat, which we consider as a model for the bulk limit. The solid lines in Fig. 1(c) depict the measured absorption coefficient for this GaSe sample at temperatures of 294 K, 180 K and 4.2 K. The curves show a pronounced shift of the absorption maximum corresponding to the direct excitonic transition and significant line broadening as a function of the sample temperature. As one of the most fundamental characterization tools, linear absorption provides valuable insight into the optical properties of a material, emphasizing especially the transitions carrying a strong dipole moment. Nevertheless, it is challenging to study with a high sensitivity the very small absorption of few-layer GaSe that is estimated to be in the order of 0.01%. To monitor the changes in the optical properties of few-layer GaSe, we therefore employ transient absorption spectroscopy. This technique provides high-frequency modulation capabilities, thus enabling us to detect precisely relative changes in the probe transmission with a sensitivity level better than 10^{-5} . For this reason, we perform degenerate pump-probe experiments, where the pump excites electronic transitions well above the bandgap and the probe detects the changes occurring at photon energies overlapping with the bandgap and related excitonic resonances.

The differential transmission spectrum at a fixed temporal delay between pump and probe pulse is plotted in Fig. 3. The observed signal results from broadening, shift and bleaching of

the excitonic transition, induced by excited carriers renormalizing the bandgap, enhancing the interband dephasing and screening the Coulomb interaction (broadening and shift) and reducing the probability for further probe photon absorption (bleaching) [22,23]. The signals appear as a modulation of optical transmission at the band edge. Panels (a) and (b) of Fig. 3 display datasets acquired at temperatures of 180 K and 4.2 K respectively, to assess the effect of line broadening. It appears that renormalization is dominant at low temperature with a derivative-like differential spectrum. Instead, bleaching is more significant at 180 K since at this temperature the excitonic line is already broad and displays as enhanced transmission, i.e. positive $\Delta T/T$, of the probe spectrum. After a quasi-instantaneous onset of the differential transmission due to carrier generation, the temporal evolution of the signal is dominated by the recombination of photoexcited carriers that occurs within few hundreds of picoseconds.

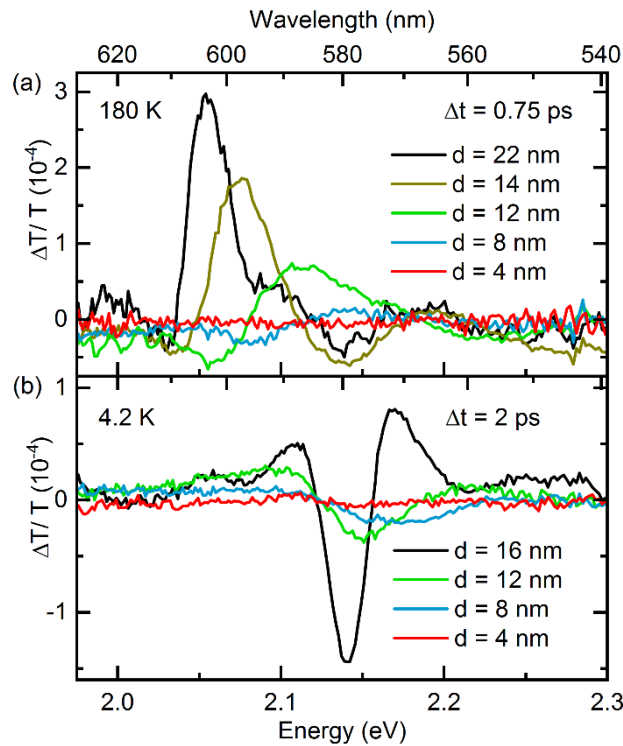


Fig 3: Relative transmission change $\Delta T/T$ after optical excitation of few-layer GaSe at (a) 180 K and (b) 4.2 K for a set of samples with different thickness d .

Independently of the spectral shape of the differential transmission, we observe in Fig. 3 a broadening and blue-shift of the excitonic signature as well as a reduction in its strength by decreasing the number of GaSe layers. Remarkably, the evolution of the signal is rather abrupt for samples thinner than 15 nm with a two-fold reduction of its amplitude when reducing the sample from 14 nm to 12 nm at 180 K and of five times between 16 nm and 12 nm at 4.2 K. For thicknesses below 8 nm the differential transmission change is no longer detectable even with our sensitive method, indicating the suppression of excitonic absorption. Fig. 4 depicts the blue-shift of the photon energy associated with the exciton transition as extracted by the pump-probe measurements at different temperatures and as a function of the GaSe sample thickness.

A similar reduction in signal strength, as observed in our measurements, was very recently reported for the photoluminescence of GaSe and attributed to rapid oxidation of thin flakes [24]. In contrast, we prevent oxidation of some samples by passivating them with a layer of Si_3N_4 right after exfoliation. Both sample sets, with and without passivation, display the vanishing signal at excitonic transitions, thus excluding oxidation as its origin. Instead, we attribute the observed behavior to a fundamental shaping of the valence band structure [25] in few-layer GaSe, as explained in the following.

The band structure of single-layer GaSe has been calculated and studied thoroughly [14,25-27], and band calculations for few-layers have been performed both for the β -GaSe polytype [25] and the ϵ polytype [28]. For the ϵ -GaSe polytype, which is relevant for exfoliated samples [29], we perform ground-state electronic structure calculations using density functional theory (DFT) within the local density approximation (LDA) [30], as implemented in the open-source package QUANTUM ESPRESSO [31]. We employ a plane-wave basis set with a kinetic energy cutoff of 80 Ry and a charge-density cutoff of 320 Ry together with fully relativistic norm-conserving pseudopotentials [32]. For the bulk we use a Γ -centered $16 \times 16 \times 3$ k -grid. Few-layer structures are calculated by keeping the distance between periodic

images constant at 18 Å along the stacking direction [z -axis in Fig. 1(a)] and the Brillouin zones are sampled with a $12 \times 12 \times 1$ k -grid centered at the Γ point. Geometries are subsequently optimized by using the Broyden-Fletcher-Goldfarb-Shanno algorithm until the net force on atoms is less than 10^{-4} N Ry/a.u. and the total energy change is below 10^{-6} N Ry, where N is the number of GaSe layers in our supercell. Spin-orbit coupling (SOC) does not play a major role in geometry optimizations, so we omit it in this step to save computational resources. However, SOC is later included in the band structure calculations.

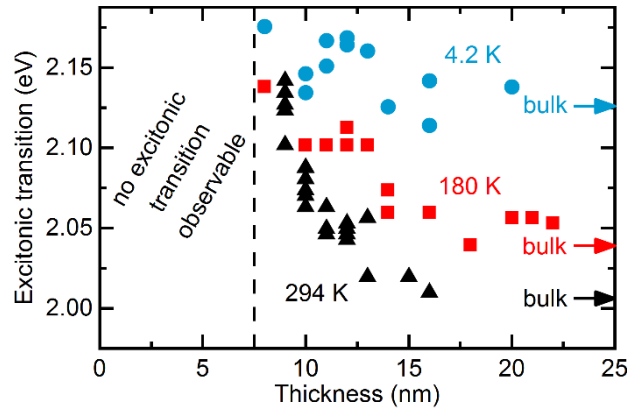


Fig 4: Measured energy position of the largest transmission change after optical excitation for different GaSe areas with thicknesses ranging from 8 to 25 nm and at a temperature of 4.2 K (blue circles), 180 K (red squares) and 294 K (black triangles). The arrows mark the energy of the exciton transition in bulk samples at those temperatures.

The evolution of the highest valence band (HVB) and the lowest conduction band (LCB) is shown in Fig. 5(a). Since splittings of the bands around the Γ point are small, only one spinor-component is displayed. Similar to previous reports [25,28], our calculations show that the HVB evolves from a parabolic shape to an inverted Mexican hat by reducing the number of layers. In this process, the effective mass of the holes changes from positive to negative at the Γ point. This transition occurs at the critical value of 8 layers, where the HVB is approximately flat around the center of the Brillouin zone. In contrast to the HVB, the

curvature of the LCB is qualitatively unaffected by the GaSe thickness, showing a parabolic shape equivalent to a positive effective mass of the electrons. As shown in Fig. 5(b), the gap between the LCB and HVB at the Γ point increases with decreasing layer thickness, as expected from quantum confinement effects due to dimensionality reduction.

We investigate further the absorption spectra of the layers by computing the complex dielectric function $\varepsilon(E) = \varepsilon_1(E) + i\varepsilon_2(E)$ within the random phase approximation (RPA) using QUANTUM ESPRESSO [31]. While we neglect excitonic effects in this approach, we can concentrate on vertical transitions within the single particle band structure, leading to noninteracting electron-hole pairs. We find that without SOC transitions from the HVB to the LCB at the Γ point are strictly forbidden in all structures of the ε -GaSe polytype independent of layer thickness, if the light is polarized in-plane. Selection rules are changed, however, with the inclusion of SOC, making such transitions weakly allowed, as has been pointed out for the bulk and single-layer cases [15,33]. We note that stacks with even layer numbers possess point-group symmetry C_{3v} , while those with an odd number are of D_{3h} symmetry. In the RPA calculations we use a $50 \times 50 \times 1$ k -grid to obtain the in-plane (straight lines) and out-of-plane (dashed lines) components of the imaginary part of the dielectric function $\varepsilon_2(E)$, as depicted in Fig. 5(c), which is proportional to the absorption coefficient. The absorption spectra are normalized to a single layer by plotting $\varepsilon_2^{(1)}(E) = L\varepsilon_2(E)/L_s$, where L_s is the thickness of the GaSe sample and L is the total thickness of the supercell perpendicular to the stack, thus also including the surrounding vacuum.

Fig. 5(c) shows that, within our assumption of noninteracting electrons and holes, the absorption of the individual layers does not change significantly as the number of layers in the GaSe crystal is reduced and that it is stronger if the light is polarized out-of-plane. However, the strongly focused beams employed in the experiments access both components of the

absorption spectrum with negligible dependence of the differential transmission signal on the angle of incidence onto the samples.

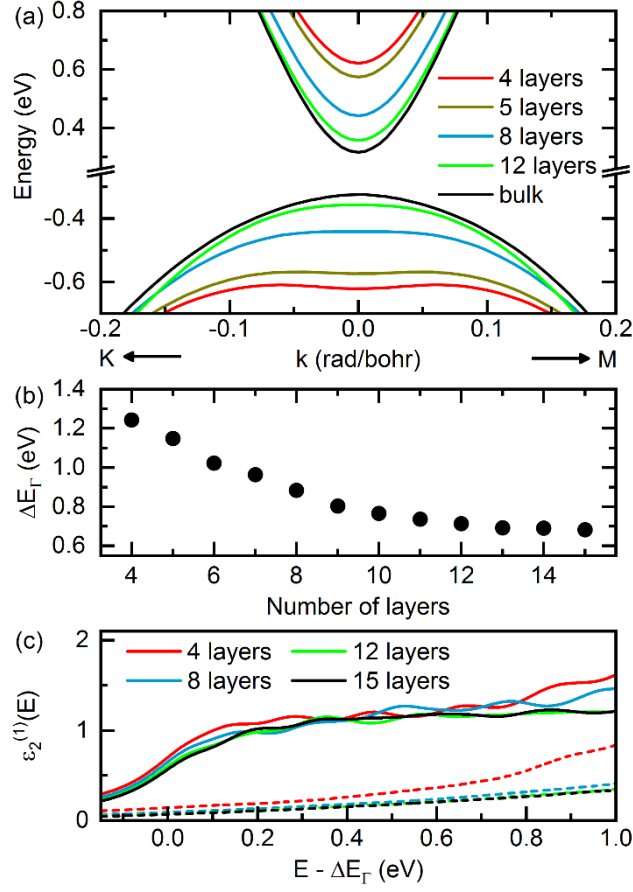


Fig 5: (a) Evolution of HVB and LCB with increasing number of layers for the ϵ -GaSe polytype. (b) Change of the DFT bandgap at the Γ point. (c) Absorption spectra of 4, 8, 12 and 15 layers calculated within RPA as a function of the photon energy. The spectra are plotted relative to the bandgap at the Γ point and are normalized to a single layer, as described in the text. Solid lines show $\epsilon_2^{(1)}(E)$, if the light is polarized out-of-plane [$\epsilon_{2,zz}^{(1)}(E)$], dashed lines are for the in-plane direction [$\epsilon_{2,xx}^{(1)}(E) = \epsilon_{2,yy}^{(1)}(E)$, see Fig. 1].

Since qualitative changes of the absorption based on band structure effects can be excluded in a single-particle picture [see Fig. 5(c)], the ab-initio calculations allow us to explain the suppression of the excitonic transition in the experiment as follows. By thinning down the GaSe nanosheets, the excitons eventually transition from the bulk to a 2D regime. This

evolution can be quantified in terms of the slab thickness d and the ground-state exciton radius R_0 : Once $d \leq 2R_0$ the 3D exciton does not fit the out-of-plane dimension anymore and hence must be considered as a 2D entity. Assuming an anisotropic hydrogenic model for Wannier-Mott excitons [34], we can deduce the relation between the exciton binding energy and the exciton radius as $R_0 = e^2 / (2\sqrt{\varepsilon_{\parallel}\varepsilon_{\perp}}E_0)$. Using literature values [35] for the exciton binding energy in bulk GaSe of $E_0 = 19.7$ meV as well as for out-of-plane and in-plane dielectric constants $\varepsilon_{\parallel} = 6.18$ and $\varepsilon_{\perp} = 10.6$, respectively, yields $R_0 = 4.5$ nm. Hence, we can expect a critical thickness of the nanosheet of approximately 9 nm. When approaching the critical regime, the binding energy increases substantially and in the ultimate 2D limit of a monolayer it should reach a value four times higher than that of the bulk exciton, assuming that the interaction potential does not change. The actual increase observed in different 2D semiconductors is even larger [36,37] because of the reduced dielectric screening [38]. Importantly, at the same thickness at which the exciton should transition from bulk to 2D characteristics, the HVB of GaSe changes from a parabolic form to the inverted Mexican hat shape. In this situation, the 2D Coulomb potential cannot bind electron-hole pairs anymore, implying that direct excitons cease to exist in GaSe with less than 8 layers of thickness. This is evident from the vanishing of the excitonic absorption peak for GaSe flakes that are thinner than 8 nm.

The energy shift of the main excitonic feature in Fig. 4 is due to the increasing energy gap between the CBM and VBM as is qualitatively confirmed by the values calculated in Fig. 5(b), where the typical underestimation of the DFT bandgap has to be taken into account [39]. Remarkably, the excitonic transitions depicted in Fig. 3 show that the blue-shift is accompanied by a broadening of the line occurring between 12 and 8 layers, emphasizing the softening of the exciton binding towards its suppression in even thinner flakes.

In conclusion, by performing highly sensitive differential transmission measurements in GaSe, we followed the change of the optical absorption from bulk to the 2D case and

observed the suppression of excitonic transitions when the number of layers is smaller than the critical value of 8. We were able to assign this behavior to a fundamental change in the band structure that leads to the formation of a valence band shaped as an inverted Mexican hat in thin GaSe, which is confirmed by our ab-initio modelling. We emphasize that the modulation of the optical properties of GaSe is intrinsic and does not require control via external parameters like substrate material or applied electric field. Thus, the discovery of this mechanism paves the way towards devices employing a single material with engineered topology, where the layer number determines the properties of light-matter interaction and complex adjacent functionalities can be integrated on a single chip.

ACKNOWLEDGMENTS

D.B. acknowledges financial support from the Emmy Noether program (BR 5030/1-1) of the German Research Foundation (DFG). D.Y. and F.P. thank the Carl Zeiss Foundation as well as the Collaborative Research Center (SFB) 767 of the German Research Foundation (DFG) for funding. M.T. is supported by the Director's Senior Research Fellowship from the Centre for Advanced 2D Materials at the National University of Singapore. Part of the numerical modeling was performed using the computational resources of the bwHPC program, namely the bwUniCluster and the JUSTUS HPC facility.

REFERENCES

- [1] S. A. Wolf *et al.*, *Science* **294**, 1488 (2001).
- [2] K. S. Novoselov *et al.*, *Nature* **438**, 197 (2005).
- [3] F. Bonaccorso, Z. Sun, T. Hasan, and A. C. Ferrari, *Nat. Photonics* **4**, 611 (2010).
- [4] K. S. Novoselov, A. Mishchenko, A. Carvalho, and A. H. Castro Neto, *Science* **353**, aac9439 (2016).
- [5] K. F. Mak *et al.*, *Phys. Rev. Lett.* **105**, 136805 (2010).
- [6] A. Molina-Sánchez *et al.*, *Phys. Rev. B* **88**, 045412 (2013).
- [7] F. Junginger *et al.*, *Opt. Lett.* **35**, 2645 (2010).
- [8] O. Schubert *et al.*, *Nat. Photonics* **8**, 119 (2014).
- [9] D. J. Late *et al.*, *Adv. Mater.* **24**, 3549 (2012).
- [10] P. Hu *et al.*, *ACS Nano* **6**, 5988 (2012).
- [11] Y. Cao *et al.*, *Sci. Rep.* **5**, 8130 (2015).

- [12] Y. Tang *et al.*, Phys. Rev. B **91**, 195429 (2015).
- [13] Y. Tang, K. C. Mandal, J. A. McGuire, and C. W. Lai, Phys. Rev. B **94**, 125302 (2016).
- [14] T. Cao, Z. Li, and S. G. Louie, Phys. Rev. Lett. **114**, 236602 (2015).
- [15] E. Mooser and M. Schlüter, Nuovo Cim. B **18**, 164 (1973).
- [16] M. Schlüter, Nuovo Cim. B **13**, 313 (1973).
- [17] S. Lei *et al.*, Nano Lett. **13**, 2777 (2013).
- [18] D. J. Late *et al.*, Adv. Func. Mater. **22**, 1894 (2012).
- [19] V. Capozzi, L. Pavesi, and J. L. Staehli, Phys. Rev. B **47**, 6340 (1993).
- [20] R. Le Toullec, N. Piccioli, and J. C. Chervin, Phys. Rev. B **22**, 6162 (1980).
- [21] A. Grupp *et al.*, J. Opt. **20**, 014005 (2018).
- [22] C. Ferrer-Roca *et al.*, J. Appl. Phys. **85**, 3780 (1999).
- [23] S. Schmitt-Rink, D. S. Chemla, and D. A. B. Miller, Adv. Phys. **38**, 89 (1989).
- [24] D. Andres-Penares, A. Cros, J. P. Martinez-Pastor, and J. F. Sanchez-Royo, Nanotechnology **28**, 175701 (2017).
- [25] D. V. Rybkovskiy, A. V. Osadchy, and E. D. Obraztsova, Phys. Rev. B **90**, 235302 (2014).
- [26] D. V. Rybkovskiy *et al.*, Phys. Rev. B **84**, 085314 (2011).
- [27] V. Zólyomi, N. D. Drummond, and V. I. Fal'ko, Phys. Rev. B **87**, 195403 (2013).
- [28] X. Li *et al.*, Sci. Rep. **4**, 5497 (2014).
- [29] N. C. Fernelius, Prog. Cryst. Growth Charact. Mater. **28**, 275 (1994).
- [30] J. P. Perdew and A. Zunger, Phys. Rev. B **23**, 5048 (1981).
- [31] P. Giannozzi *et al.*, J. Phys.: Cond. Mat. **21**, 395502 (2009).
- [32] N. Troullier and J. L. Martins, Phys. Rev. B **43**, 1993 (1991).
- [33] P. Li and I. Appelbaum, Phys. Rev. B **92**, 195129 (2015).
- [34] J. J. Hopfield and D. G. Thomas, Phys. Rev. **122**, 35 (1961).
- [35] O. Madelung, *Semiconductors: Data Handbook* (Springer, Berlin, 2004).
- [36] B. Zhu, X. Chen, and X. Cui, Sci. Rep. **5**, 9218 (2015).
- [37] H. M. Hill *et al.*, Nano Lett. **15**, 2992 (2015).
- [38] L. Keldysh, JETP Lett. **29**, 658 (1979).
- [39] R. M. Martin, *Electronic Structure: Basic Theory and Practical Methods* (Cambridge University Press, Cambridge, 2004).